4th URSI AT-RASC, Gran Canaria, 19-24 May 2024

Imaging Microburst Precipitation with Atmospheric X-ray emissions (IMPAX) CubeSat Mission

Chris A. Colpitts[1], Robert Marshall[2], Harlan Spence[3], Aaron Breneman[4], Lindsay Glesener[1], Sadie Elliott[1]
(1) University of Minnesota, Minneapolis, MN; (2) University of Colorado, Boulder, CO; (3) University of New Hampshire, Durham, NH; (4) NASA Goddard Space Flight Center, Greenbelt, MD

Abstract

The Imaging Microburst Precipitation with Atmospheric X-ray emissions (IMPAX) CubeSat was recently selected by NASA's H-FORT program, with a planned launch date of late 2027. The overarching goal of IMPAX is to quantify relativistic electron microburst precipitation as a radiation belt loss mechanism.

1. Introduction

Microbursts are highly localized precipitation events of keV-MeV electrons lasting 10s to 100s of ms. They are observed at low altitude on magnetic field lines mapping to the outer radiation belt, most often during the main phase and early recovery phase of geomagnetic storms. They are known to be a significant loss mechanism for outer belt electrons during storm time, but the importance of microburst precipitation relative to other radiation belt loss processes has not been established. This mission will allow us to make this critical quantification by answering the following Science Questions:

1. **What is the energy distribution (flux and spectrum) of electron microburst precipitation into the Earth's atmosphere?**

2. **Where are relativistic electron microbursts that precipitate into the Earth's atmosphere generated?**

The answers to these questions will enable us to quantify this loss process to a much greater extent than previous measurements have allowed. The energy distribution will provide the flux of electrons at different energies precipitating within individual microbursts, trains of microbursts, and over the full precipitation region, as well as how this flux varies temporally (storms/substorms) and spatially (L/MLT). Identifying the generation location of microbursts will significantly constrain the spatial and temporal scale of microburst precipitation. IMPAX will determine how this generation location varies with microburst energy, for storms or substorms, and by L, MLT, or MLAT of the observed precipitation. Combining the measured energy distribution of precipitating electrons with the spatial and temporal scale of the precipitation region will determine how long it would take for microburst loss to deplete the outer radiation belt. This timescale will then be compared to the observed energy-dependent outer belt decay, which will quantify the loss that can be accounted for by microburst precipitation and thus its relative importance as a radiation belt loss process.

To answer these questions IMPAX will take the novel approach of **combining high resolution direct measurement of electrons within or near the loss cone and the first ever imaging in low-earth-orbit (LEO) of bremsstrahlung X-rays created when the precipitating electrons hit the atmosphere**. The combination of these instruments allows a precise measurement of bounce loss cone electron flux and spectrum that is not possible with only direct electron measurements at LEO, or short-duration balloon measurements of X-rays at low altitude. **The ultra-high energy resolution particle measurements will also show the energy-time dispersion that will allow identification of the microburst generation location**.

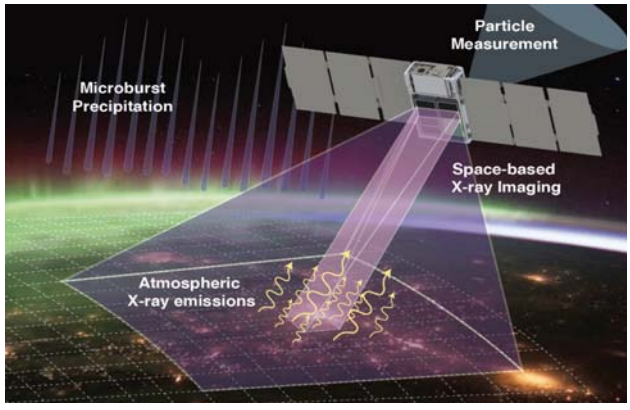

Figure 1. *IMPAX will measure microburst precipitation both by directly measuring the electrons and by imaging X-rays produced by bremsstrahlung in the upper atmosphere due to the precipitation. The direct measurement of the precipitating electrons will provide the spectra of the precipitation and the energy dispersion to determine the source location, while the X-rays provide measurements of the energy deposited by the precipitation and the size of the precipitation region.*

2. Methodology

2.1 Energy Distribution of Microburst Precipitation

IMPAX will determine the energy distribution of microburst precipitation utilizing the technique of combining images of X-rays produced by the microbursts with the direct electron measurements. This in turn will allow us to estimate the total energy deposition from the radiation belts into the atmosphere and will provide much better estimates of the global effects of microburst precipitation on both the atmosphere and radiation belts. Most previous missions are unable to resolve the loss cone, and so cannot specify the total precipitating flux. X-ray measurements are typically made with low-altitude short-duration balloon flights. However, X-ray observations from a single balloon do not provide good spatial information about the precipitating region.

IMPAX represents a significant advancement from all previous studies by providing imaging of X-Rays over a large (FOV: 930x930 km) section of the precipitation region every 50 ms throughout the radiation belt L-shells, and combining these images with direct measurements of the precipitation electrons. The spacecraft will traverse the radiation belts 4 times each ~90 minute orbit, covering all MLTs over a 6-month mission. The precipitating electron *spectrum* will be determined by the particle detector, and will be used together with the X-ray fluxes to determine the precipitating electron *flux*. Bremsstrahlung X-ray generation from high energy precipitating electrons is well understood, and techniques for inverting the process to determine the electron energy distribution have been employed with accuracy for decades and continue to be refined today [1, 2 ,3]. Combining the X-ray observations with direct measurements of the precipitating electrons further constrains the inversion process. IMPAX, with its excellent temporal resolution (50 ms cadence), will generate the first images of microbursts from LEO, and the first combination of microburst X-ray observations with high time- and energy-resolution electron measurements. **Together, these new measurements, which can only be performed on a CubeSat at LEO with this instrumentation, will quantify the loss due to microburst electron precipitation from the radiation belts**.

Figure 2 demonstrates the image reconstruction method with our coded aperture design. At left, two point sources are introduced, simulating two microbursts separated by ~200 km, with the associated X-rays originating from ~50 km altitude. These X-rays are propagated back to the spacecraft at 500 km altitude, and through the instrument as modeled in GEANT4. X-ray counts hitting the detector pixels are collected, along with artificial Poisson noise that represents the space radiation background environment. Next, the first step of image reconstruction is to decode the recorded image using the coded aperture anti-mask (i.e. deconvolution). Image ringing due to the imperfect point-spread function is then removed using Lucy-Richardson deconvolution, which, in addition to other cleaning procedures, yields the final image reconstruction shown below the source image. This example demonstrates the point-spread function of the instrument, and also shows the ability of the instrument to distinguish multiple signal peaks. The example on the right of Figure 2 shows similar results for a "band" of precipitation spanning the instrument FOV. In both cases the source distribution is well estimated, though edge smearing is evident.

These images of observed X-ray emission are then used, in combination with the direct electron measurements, to determine the precipitating electron flux and spectrum in the following manner [3]. The observed photon spectrum is fit with a linear combination of detector responses to mono-energetic electron beams. Every possible combination of coefficients is tested, and the best-fit is found based on the minimization of squared residuals. This inversion procedure was tested on a wide range of different input distributions, including exponential, mono-energetic, uniform, and power-law distributions, each showing good inversion results.

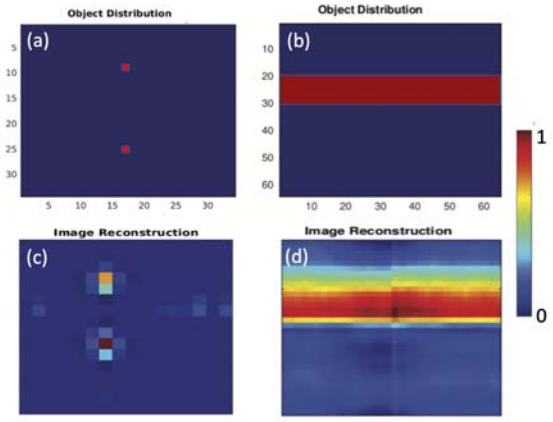

Figure 2. *Demonstration of two different source functions (top panels) and their coded aperture final image reconstruction (bottom panels). (a, c) two point sources emulating small (50 km) patches of precipitation and their zoomed-in image reconstruction, respectively. (b,d) a band of precipitation spanning one dimension of the FOV and its reconstructed image. Axes are integer pixel numbers and the colorbar scale is in normalized arbitrary units.*

For IMPAX, the energy distribution will be further constrained by the I-FIRE instrument. This constrained inversion technique was demonstrated in [4] using a measured energy distribution with some uncertainty, as would be measured by I-FIRE. Fits from FIREBIRD data [5, 6] reveal an exponential energy distribution. These distributions of microburst precipitation were forward-modeled into the atmosphere, producing X-ray fluxes at the IMPAX altitude of 500 km. The X-ray flux was then used to estimate the precipitation flux, following the method of [3]. For all distributions, the error in the estimated flux was found to be no more than 20%, and lower for higher E_0 due to a larger number of X-rays produced. These results demonstrate that IMPAX measurements can be used to accurately determine the energy distribution of microburst precipitation. **IMPAX will thus provide the most accurate estimates of the precipitating microburst electron distribution ever measured.** The spatial and

temporal scales of the full precipitation region will also be determined both by identifying the generation location and from covering all L-shells, MLT, and geomagnetic conditions during the course of the mission. The I-AXIS imager will determine the flux of microbursts through every region within this overall precipitation region, and give the spatial scale and temporal duration of microburst trains/clusters. **Together, the directly measured precipitation and images of X-ray emissions within a given region will provide the total flux and spectrum of microburst precipitation in that region.** This will then be extrapolated to the spatial and temporal extent of the full precipitation region to determine the total atmospheric loss due to microbursts, which will be compared with observed losses to determine the relative importance of microburst precipitation as a radiation belt loss process.

2.2 Microburst Source Location

IMPAX will use the direct measurements of precipitating electrons to identify and constrain the location and properties of the microburst generation region. Within a given magnetic meridian (single MLT) it is possible to identify the location of microburst generation using observed energy-time dispersion. This arises from the frequency- and energy-dependent differences in both the travel time of the emitted whistler mode wave and the time it takes the electrons to propagate along the magnetic field line to the LEO satellite. This total travel time is dependent on the location of the chorus source (assumed near-equatorial), propagation characteristics (ducted or unducted), emission characteristics (frequency, wave normal angle), and the location of resonance scattering. Unfortunately, due to the low energy resolution of previous measurements including FIREBIRD, only a handful of microbursts exhibiting likely energy/time dispersion have been observed (e.g. Figure 3a). *IMPAX I-FIRE will have flexible binning of energies, with 64 energy bins covering 125-1000 keV that can then be recombined on the ground.* As we show below, this is sufficient energy resolution to accurately quantify energy/time dispersion on observed microbursts, allowing us to determine their source with a ray-tracing technique. For this example, in Figure 3 we compare the dispersion of a weak microburst observed by the 5-bin FIREBIRD 3 collimated detector to the dispersion that would be observed in the same microburst with a 64-bin simulated IMPAX I-FIRE detector, which includes an improved lower energy range of 125 keV. We simulate a microburst in energy and time as $J_0\exp(-(E/E_0)^n)*\exp(-(t-dt)^2/t_0^2)$. Parameters were chosen so that the response of the *simulated* 5-bin detector (red curves, lower right four panels) matched the *real* response (black curves). For this microburst, the best fit occurs with n=1.2, E_0=100 keV, dt=0.47 sec, t_0=0.1 sec, J_0 = 25/(cm^2-s-str-keV). From this functional form we can recreate this microburst with high fidelity in energy and time.

Given this functional form of the observed microburst, we can then apply it to a simulated IMPAX detector with any desired number of energy bins at any energies to investigate what I-FIRE would observe with that energy resolution. The energy dispersion in both these simulated high-resolution observations and the actual 5-bin FIRE observations are then used to calculate the range of possible locations this microburst could have come from to create the observed dispersion profile. This will allow us to determine what energy resolution would have been required to identify the microburst generation location for this event. The full-fidelity microburst can be input into a simulated I-FIRE detector with any desired number of energy channels and a 20 msec cadence (compared to 50 msec of FIREBIRD). As we will show, the resulting energy dispersion can then be used to accurately identify the microburst source. By comparison, the original 5-bin FIRE observations cannot identify the source.

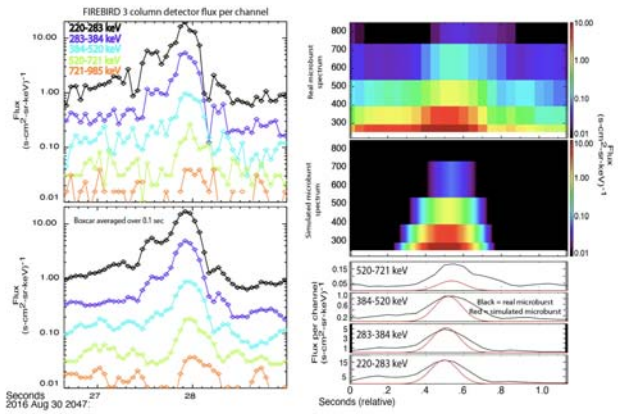

Figure 3*: Simulated microburst based on a FIREBIRD dispersive microburst. The left column shows the full resolution and boxcar averaged microburst flux for the 5 onboard detector channels. The right column shows spectrograms of the real microburst and simulated microburst following simulated re-detection by the FIREBIRD instrument, as well as their channel-by-channel comparison for energies up to 721 keV.*

Figure 4 shows an energy vs time comparison of the simulated microburst as detected by FIRE (5 bins, panel a), and I-FIRE (16 and 64 bins in panels b,c). Energy error bars represent the width of each detector energy bin, and time error bars are the width of the samples (50 msec for FIRE and 20 msec on I-FIRE) or larger depending on an error metric based on the signal-to-noise ratio. From these errors, a chi square minimization technique was used to determine a best fit line (black), with maximum and minimum possible line fits (red) determined from the one-sigma values of the best fit slope and intercept. Comparison of the two extreme fits for each plot gives the range of possible differences in microburst arrival time at FIRE vs. I-FIRE for two given energies. The I-FIRE detector has a much smaller uncertainty than the I-FIRE detectors, even in nominal mode using 16 energy bins.

The large delta-time uncertainties associated with the 5-bin detector mean that the FIRE detector *fundamentally cannot* constrain the location within the latitudinal region where these energies are cyclotron resonant. This detector also cannot distinguish between

sources in the northern and southern hemisphere, and hence cannot distinguish between +/- cyclotron resonances. However, the smaller uncertainties associated with the I-FIRE 16-bin nominal mode and 64-bin burst mode data indicate that the microbursts are created from n=-1 *regular* cyclotron resonance in the northern hemisphere at magnetic latitudes from 27-35 deg magnetic latitude along the L=6 field line. A similar analysis can be done for higher order cyclotron resonances |n|> 1 and for ducted propagation.

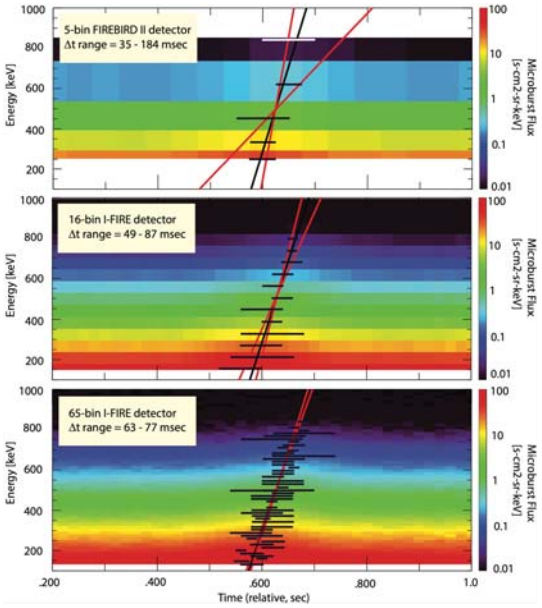

Figure 4*: The simulated microburst as detected by the FIRE (panel a) and I-FIRE detector with 16 and 64 bins (panels b,c). Each panel shows the best-fit line (black) and error slopes (red) corresponding to errors in time (black error bars) and energy (energy bin width). The max and min error slopes are used to determine a range of delta-time of arrival differences (inset panels) at a simulated LEO CubeSat at L=6. These are used to identify the location of the microburst source and chorus source properties with a ray tracing analysis.*

In addition to identifying the microburst source, this type of simulation can be repeated for a range of equatorial source locations and emission frequencies to ascertain the chorus source extent and properties. Simulating a range of frequencies from 300-1300 Hz and a range of equatorial chorus source locations from L=5-8 we find that with the 5-bin solution from the FIRE instrument possible source locations vary widely from L=5.6 to 6.9, with emission frequencies from 600-1000 Hz. Using the 16-bin (nominal mode) I-FIRE solution is vastly better and narrows the source locations from L=6 to 6.5 and the source emission to only 1000 Hz. By comparison, the *only* solution for the burst 64-bin (burst mode) fit is 1 kHz emission at L=6.15. This same ray-tracing technique can be used to determine the wave normal angles of the causative chorus emissions. Thus, the dispersive properties identified from the high-resolution I-FIRE instrument will allow determination of chorus source properties producing the microbursts.

This example shows that the increased energy resolution of the I-FIRE detector enables a determination of the source location and cyclotron resonance condition of the microburst region, and the location and properties of the causative chorus source. FIREBIRD data, and simulations [7] have also indicated that microburst dispersion is not always linear, but can take on a number of curves including "boomerang" curves where intermediate energies arrive before the highest and lowest energies. These unique signatures will allow a further narrowing of the chorus source and scattering regions. **IMPAX will therefore provide the source location, as well as source chorus location and key emission properties, of a large number of microburst events observed with a variety of dispersive signatures, across the entire precipitation region and during the full range of geomagnetic conditions.** This resulting database will provide a significantly improved understanding of the microburst generation process, including analysis of the statistical connection between chorus source properties and microbursts.

References

[1] Millan, R. M., et al. (2013), The Balloon Array for RBSP Relativistic Electron Losses (BARREL), *Space Sci. Rev.*, 179, 503‐530, doi:10.1007/s11214-013-9971-z.

[2] Woodger, L. A. et al (2015), A summary of the BARREL campaigns: Technique for studying electron precipitation, *J. Geophys. Res. Space Physics*, 120, 4922‐4935, doi:10.1002/2014JA020874.

[3] Xu, W., & Marshall, R. A. (2019). Characteristics of energetic electron precipitation estimated from simulated bremsstrahlung X-raydistributions. *J. Geo. Res.,* 124, 2831‐2843. https://doi.org/10.1029/2018JA026273

[4] Marshall, Robert A., et al (2020), The AEPEX mission: Imaging energetic particle precipitation in the atmosphere through its bremsstrahlung X-ray signatures, Advances in Space Research, 10.1016/j.asr.2020.03.003.

[5] Crew, A. B. et al (2016). First multipoint in situ observations of electron microbursts: Initial results from the NSF FIREBIRD II mission. *J. Geo. Res.* 121, 5272‐5283. https://doi.org/10.1002/2016JA022485

[6] Breneman, A. et al. (2017). Observations directly linking relativistic elec-tron microbursts to whistler mode chorus: Van Allen Probes and FIREBIRD II. Geophysical Research Letters, 44, 11,265-11,272. https://doi.org/10.1002/2017GL075001

[7] Saito, S., Miyoshi, Y., & Seki, K. (2012). Relativistic electron microbursts associated with whistler chorus rising tone elements: GEMSIS-RBW simulations. *J. Geo. Res.* **117**, A10206. https://doi.org/10.1029/2012JA018020